Fully Automated Muscle Ultrasound Analysis (MUSA): Robust and Accurate Muscle Thickness Measurement

Submitted to UMB

Fully automated Muscle UltraSound Analysis (MUSA): robust and accurate muscle thickness measurement

Cristina Caresio[1], Massimo Salvi[1], Filippo Molinari[1], Kristen M. Meiburger[1], and Marco Alessandro Minetto[2,3]

[1]Biolab, Department of Electronics and Telecommunications, Politecnico di Torino, Turin, Italy

[2]Division of Physical Medicine and Rehabilitation, Department of Surgical Sciences, University of Turin, Turin, Italy

[3]Division of Endocrinology, Diabetology and Metabolism, Department of Medical Sciences, University of Turin, Turin, Italy

SHORT TITLE
Muscle UltraSound Analysis (MUSA)

CORRESPONDING AUTHOR
Prof. F. Molinari, PhD
Biolab, Department of Electronics and Telecommunications, Politecnico di Torino, Torino, Italy.
Corso Duca degli Abruzzi, 24 - 10129 Torino, ITALY
Phone: 0039 011 090 4153
Fax: 0039 011 090 4217
E-mail: filippo.molinari@polito.it

ABSTRACT

Musculoskeletal ultrasound imaging allows non-invasive measurement of skeletal muscle thickness. Current techniques generally suffer from manual operator dependency, while all the computer-aided approaches are limited to be semi-automatic or specifically optimized for a single muscle. The aim of this study was to develop and validate a fully automatic method, named MUSA (Muscle UltraSound Analysis), for measurement of muscle thickness on longitudinal ultrasound images acquired from different skeletal muscles. The MUSA algorithm was tested on a database of 200 B-mode ultrasound images of rectus femoris, vastus lateralis, tibialis anterior, and medial gastrocnemius. The automatic muscle thickness measurements were compared to the manual measurements obtained by three operators. The MUSA algorithm achieved the 100% segmentation success rate; with mean differences between the automatic and manual measurements in the range 0.06 – 0.45 mm, MUSA performance was statistically equal to the operators and its measurement accuracy was independent on the muscle thickness value.

Keywords: Muscle ultrasonography, musculoskeletal ultrasound, automatic muscle thickness measurements

INTRODUCTION

Musculoskeletal ultrasound imaging enables to non-invasively measure parameters reflecting skeletal muscle size. Muscle thickness measurement has been extensively used in both physiological and clinical studies to investigate the adaptations in muscle size occurring with training (i.e., muscle hypertrophy, Narici et al. 2011, Seynnes et al. 2013), disuse atrophy (de Boer et al. 2008), ageing (i.e., primary sarcopenia, Narici et al. 2003, Atkinson et al. 2010, Agyapong-Badu et al. 2014), and pathological conditions (Pillen et al. 2008). Moreover, a number of studies adopted muscle thickness measurement to predict leg skeletal muscle mass (Takai et al. 2013) and total body fat free mass and muscle mass (Abe et al. 2015; Takai et al. 2014), as well as to indirectly assess muscle volume and cross-sectional area in extremity and trunk muscles (Abe et al. 2016; Akagi et al. 2010; Esformes et al. 2002; Ogawa et al. 2012; Takai et al. 2011). In most of the previous studies, muscle thickness values were obtained by measurements performed in triplicate on one scan (i.e., muscle thickness was obtained as the average of three measurements performed in the proximal, central, and distal positions of the scan) by one (or more) operator(s) and repeated on the same image on a separate day by the same operator(s) to provide evidence of low typical errors and high intra-class correlation coefficients (Atkinson et al. 2010; Caresio et al. 2014; Esformes et al. 2002; Narici et al. 2003; Seynnes et al. 2013). However, the visual identification of the profiles of the superficial and deep aponeuroses and the "manual" measurement of muscle thickness are time consuming and prone to errors.

In recent years, several computer-aided approaches have been proposed to measure muscle thickness on ultrasound images. Koo et al. (2010) proposed a muscle boundary tracking algorithm to track the locations of aponeuroses and measure the thickness of the

pectoralis major muscle. Wong et al. (2012) proposed a sequential quadratic programming approach (based on a novel log-Rayleigh likelihood function) followed by the identification of the regions of interest to measure the thickness of abdominal muscles. Han et al. (2013) investigated the performance of two preprocessing procedures (aimed to enhance the aponeurotic hyperechoic regions over the speckles) which could help the automatic estimation of the gastrocnemius muscle thickness based on Revoting Hough Transform. Finally, Ling et al. (2013) proposed a method to extract the aponeuroses boundaries and calculate the gastrocnemius muscle thickness as the distance between the lower boundary of superficial aponeurosis and upper boundary of deep aponeurosis.

A major limitation of all these approaches is that they are specifically optimized for a single muscle or manually driven (i.e., they consist in semi-automatic approaches that still require user input to provide a set of starting points), or both, making them unsuitable for clinical use. To the best of our knowledge, no previous study proposed a fully automatic method for the measurement of the thickness of different superficial skeletal muscles. Therefore, the aim of this study was to develop and validate a fully automatic method for measurement of muscle thickness on ultrasound images acquired from different skeletal muscles.

MATERIALS AND METHODS

Subjects

Fifty healthy subjects of both genders (25 males and 25 females, mean ± SD age: 31.0 ± 10.9 years; body mass index: 24.3 ± 4.7 kg /m^2) volunteered to participate in the study. They were free from neuromuscular or skeletal impairments. The subjects received a detailed

explanation of the study and gave written informed consent prior to participation. The study was conducted at the Division of Endocrinology, Diabetology and Metabolism, Department of Medical Sciences, University of Turin, Italy, was conformed with the guidelines in the Declaration of Helsinki and was approved by the local ethics committee.

Ultrasound procedures and equipment

Ultrasound B-mode images of the following four muscles were acquired in each subject during a single experimental session: rectus femoris, vastus lateralis, tibialis anterior, and medial gastrocnemius. The dominant side was investigated.

The same sonographer (MAM, 5 years of experience in musculoskeletal ultrasound imaging) performed all assessments. Each muscle was acquired in the longitudinal plan, and a total of 200 images (50 subjects x 4 muscles) were captured and analysed. To ensure the optimal representation of the different muscles, we adopted the following criteria: *i)* rectus femoris: we optimized the representation of the superficial and deep aponeuroses; *ii)* vastus lateralis and medial gastrocnemius: we optimized the representation of the superficial and deep aponeuroses and of the muscle fascicles; *iii)* tibialis anterior: we maximized the representation of the bone boundary and of the muscle fascicles.

Images of the medial gastrocnemius were acquired with the subjects in the prone position, whereas for all other muscles subjects were positioned supine. In all measurements, the lower limb joints were extended and the subjects were asked to completely relax their muscles. A suitable amount of ultrasound coupling gel was used to ensure optimal image quality and to minimize the transducer pressure on the skin. According to previous studies (Arts et al. 2010; Caresio et al. 2014; Minetto et al. 2016), all scans were performed by

placing the transducer in correspondence of the largest muscle diameter at the following anatomical sites: the rectus femoris was measured half-way along the line from the anterior-superior iliac spine to the superior border of the patella; the vastus lateralis half-way along the line from the anterior-superior iliac spine to the superolateral border of the patella; the tibialis anterior at one-quarter of the distance from the inferior border of the patella to the lateral malleolus; the medial gastrocnemius from the mid-sagittal line of the muscle, midway between the proximal and distal tendon insertions.

All images were acquired using a MyLab™ Twice ultrasound device (Esaote, Genova, Italy) equipped with a linear-array transducer (code LA533) with variable frequency 3-13 MHz. The gain was set to 50% of the range, dynamic image compression was turned off, and time gain compensation was maintained in the same (neutral) position for all depths. All system-setting parameters were kept constant throughout the study and for each subject, except depth (initially set at 44 mm) that was modified during the examination (range: 44 - 59 mm) to visualize the entire muscle thickness. The images were converted in DICOM format and then transferred to a workstation for offline processing.

MUSA algorithm architecture

We named this algorithm as MUSA (Muscle UltraSound Analysis). The MUSA algorithm was designed in order to automatically detect the muscle aponeuroses in longitudinal ultrasound images. Once the aponeuroses are correctly located, the algorithm estimates the muscle thickness. The algorithm was developed using the Matlab™ (MathWorks, Natick, MA, USA) environment. A schematic description of the procedure is reported in fig. 1; the detailed description of the steps is reported in the following.

Image preprocessing

The original DICOM image (fig. 2.A) is automatically cropped to maintain only the region containing the ultrasound data. Automated cropping is obtained by relying on the DICOM header tag "RegionLocation" (Molinari et al. 2009). The uppermost 2 mm of the image are then blackened to exclude the dead zone and the skin from further processing. The automatically cropped image can be seen in fig. 2.B.

Automated search for the aponeuroses candidates

This first processing step is devoted to automatically search for the possible position of the aponeuroses inside the image. The image is first downsampled by a factor of two (i.e., the number of rows and columns of the image is halved). To enhance all the structures inside the image that are possible aponeuroses we compute the vertical Sobel gradient of the image (fig. 2.C) and then we apply a vertical First-Order Derivative Gaussian (FODG) filter to the processed image. The FODG filter is obtained by the convolution of a Gaussian kernel and a simple derivative filter (Florack et al. 1992). This filter enhances all the structures bigger than the dimension of the FODG kernel and attenuates the others. Hence, the dimension of the FODG kernel is set to 9 pixels, in order to ease the aponeurosis highlighting.

Finally, we threshold the FODG output to produce the binary FODG mask (fig. 2.D). The threshold is set the 80% of the maximum gray level of the FODG output.

As can be seen by fig. 2.D, the binary FODG mask represents the two muscle aponeuroses as well as other white regions representing different structures. A heuristic cleaning step is

performed to remove all the structures that do not match specific conditions (*i.e.*, that do not qualify as aponeuroses candidates). We label all the disconnected regions in fig. 2.D and we approximate them as ellipses. Since the structures corresponding to aponeuroses have a horizontal size similar to the size of the image, we remove all the regions with eccentricity lower than 0.995 and with a major axis shorter than 70% of the length (in pixels) of the image. The cleaned mask is shown in fig. 2.E. Branching and region filling is then performed to adjust the morphology of the remaining regions. The white arrow in fig. 2.F shows the correction made with respect to the irregularity of the superficial aponeurosis of fig. 2.E.

Selection of the actual aponeuroses

As can be seen from fig. 2.F, the binary FODG mask often contains more candidate aponeuroses. To distinguish the two actual aponeuroses from the other candidates, we check the presence of muscle fascicles between each pair of candidates (*i.e.* we check that the two aponeuroses actually delimit the muscle region). We first equalize the original image and then apply a global thresholding using the Otsu's method (Otsu 1979) to obtain a binary mask (that will be indicated in the following as "binary fascicle mask"). Figure 3.A shows the binary fascicle mask where aponeuroses and fascicles are visible. The aponeuroses candidates (fig. 2.F) are then removed from this binary fascicle mask (fig. 3.B), together with all the regions having an area lower than 10 pixels (which are likely to represent oversegmentation due to speckles).

Since the muscle fascicles are represented by a line with a specific orientation, we applied the Standard Hough Transform (Duda and Hart 1971) on the binary fascicle mask. The

Standard Hough Transform uses the parametric representation of a line in polar coordinates. The variable θ is the angle of the perpendicular projection from the origin to the line measured in degrees clockwise from the positive x-axis. The angle of the line itself is θ+90°, also measured clockwise with respect to the positive x-axis. The range of θ for our application is $-90° \leq \theta \leq 85°$. Fig. 3.C shows the original B-mode image (background) with overlaid the binary FODG mask (white) and the detected fascicles (green lines). The uppermost endpoint of each fascicle is marked by a yellow dot.

The image is then considered column-wise. We process one column every ten (decimation) until reaching the total number of columns N, since, at this stage, we do not need the accurate profile of the aponeurosis, but we just need to select the correct aponeuroses among the possible candidates. On each *i-th* column, the candidates are considered starting from the deepest. We apply an iterative heuristic search made of the following steps:

1) Considering a point of the deepest candidate (marked by X_i in fig. 3.D), we delineate a region of interest (ROI) (blue region in fig. 3.D). The vertical size of the ROI corresponds to the distance of the considered point X_i from the corresponding point on the same column belonging to the closest candidate aponeurosis upwards (marked by Y_i in fig. 3.D). The horizontal size of the ROI is fixed to 41 pixels (corresponding to 3.8 mm). This horizontal size was selected in order to make sure that the region contained some fascicles.
2) If the vertical size of this ROI is lower than 15 mm, the two candidates are too close and they cannot be the actual aponeuroses; hence, the point on the deepest candidate is discarded and the procedure goes back to point 1).

3) If the condition at point 2) is matched, the points X_i and Y_i indicate the deep and superficial aponeurosis (that will be indicated in the following as APO_{Inf} and APO_{Sup}), respectively, only if muscle fascicles are present in between. Hence, we compute the number of fascicles endpoints (yellow dots in fig. 3.C) falling into the ROI. If this number is lower than 20% of the overall number of endpoints in the whole image, we consider that there is no muscle in between X_i and Y_i. The procedure then discards X_i and steps back to 1).
4) If the number of fascicle endpoints is higher than 20% of the overall number of endpoints in the image, the point X_1 is marked as the deep aponeurosis APO_{Inf} and the point Y_1 as the temporary superficial one APO_{Sup}.
5) A further control is made on the gray level of point Y_i : if the gray level of Y_i , in the original image, is lower than the 60% of the maximum gray level found along the *i-th* column, the index of Y_i is iteratively updated proceeding from the bottom to the top along the column, until this condition is matched.
6) The procedure iterates considering all the other columns of the image (fig. 3.D).

This heuristic search outputs a series of points X_i that delineate the position of the deep aponeurosis APO_{Inf} and a series of points Y_i that delineate the superficial aponeurosis APO_{Sup}. The final result of the heuristic search is depicted in fig. 4.A. Spike detection and removal is applied to correct for possible inaccuracies and the APO_{Sup} and APO_{Inf} profiles (fig. 4.B).

Final aponeuroses tracing

As can be seen in fig. 4.B, the profile is roughly placed in correspondence of the aponeuroses, but refinement is needed. We adopt a Difference of Gaussians (DoG) filter to detect the actual edges. The DoG mask of an input image *I* can be defined as:

$$DoG = (I * G_1) - (I * G_2)$$

where G_1 and G_2 are low-pass Gaussian kernels. We set for each kernel the size *S* (dimension in pixel) and the corresponding standard deviation σ as follows: S_1 = 11 pixels, S_2 = 81 pixels, σ_1 = 101 pixels, and σ_2= 21 pixels. The DoG mask is represented in fig. 4.C. In the DoG mask, the transitions from bright to dark (*i.e.* from APO_{Sup} which is bright to muscle which is dark) are positive, whereas the transitions from dark to bright (*i.e.* from muscle to APO_{Inf}) are negative. Thus, we could locate the exact position of the interface between muscle and aponeurosis in each column of the image. Figure 4.D reports the final profiles of the superficial and deep aponeuroses, interpolated by a bicubic spline.

Tibialis anterior images

The tibialis anterior is a bipennate muscle, meaning that the muscle fibers branch out at a specific angle (i.e., pennation angle), from a central intramuscular fascia to the superficial and deep aponeurosis (Maganaris and Baltzopoulos 1999). As shown in fig. 5.A, the fascicles of the two compartments present opposite pennation. Our MUSA architecture is adaptable to the processing of images of multi-compartmental muscles, since its architecture can be repeated for every compartment of the muscle. In the specific case of the tibialis anterior muscle:

1) Considering the FODG (fig. 5.B), the processing starts from the lower compartment. Among all candidates, the ones that are likely to correspond to the deepest

aponeurosis and to the central fascia are traced (fig. 5.C) by applying the same strategy as described in the previous section.

2) The central fascia of the tibialis anterior muscle defines the bottom limit of the upper compartment. MUSA is then applied from this profile upwards, to detect the superficial aponeurosis (fig. 5.D).
3) Once the deep and superficial aponeurosis are located, the final profiles are obtained by using DoG mask (fig. 5.E).

Since the pennation changes between the two compartments, the range of *theta* for the Standard Hough Transform has been chosen as $-90° \leq \theta \leq 85°$ for the upper compartment and as $95° \leq \theta \leq 260°$ for the lower compartment.

Performance metric and statistics

MUSA was tested on the whole database of 200 B-mode ultrasound images. The automatic muscle thickness measurement was obtained by the centerline distance metric. This distance metric has previously been used for thickness measurements (Saba et al. 2012; Sheehan et al. 1986) and consists in initially determining the centerline between two boundaries. Then, for each point of the centerline, a chord perpendicular to it is plotted. The length of this chord is the measure of muscle thickness in that point. The average distance for all the chords along the centerline is the final centerline distance metric.

In addition to the automatic analysis of muscle thickness, three experienced operators independently and manually measured the muscle thickness in the same 200 images. The manual measurements were performed using the software ImageJ (National Institutes of Health, Bethesda, MD): the operators manually placed five segments between the two

muscle aponeuroses at around 10%, 30%, 50%, 70% and 90% of the entire length of the muscle profile in the image. The Euclidean distance between the end points of each segment was calculated and the final manual measurement was obtained as the average of these five distances.

The automatic muscle thickness measurements were compared to the manual measurements obtained by the three operators for each muscle. The comparison was performed by using the Kruskall-Wallis ANOVA (followed by Dunn's post hoc test) and the intraclass correlation coefficient ICC (2,1). Finally, the manual and automatic measurements were compared using the Bland-Altman plot (Bland and Altman 1990). To assess the existence of a statistical dependence between the two data sets, a correlation analysis between the differences and averages of the two measurement methods (x and y axis of the Bland-Altman plot) was also performed using the Spearman test.

Data were expressed as mean ± standard deviation (SD). Threshold for statistical significance was set to $P = 0.05$. ICC analysis was performed with SPSS 20.0 (SPSS Inc., Chicago, IL, USA) software package, while all other statistical tests were performed with Statistica 6 (Statsoft Inc., Tulsa, OK, USA) software package.

RESULTS

Segmentation results

Left panels of Fig. 6 shows the segmentation performance of the MUSA algorithm on representative images of all muscles studied: rectus femoris (fig. 6.A), vastus lateralis (fig. 6.C), tibialis anterior (fig. 6.E), and medial gastrocnemius (fig. 6.G). Similar to these representative examples, the MUSA algorithm detected the aponeurosis profiles, and

therefore automatically calculated the muscle thickness, in the whole database of 200 images (100% segmentation success rate).

Performance evaluation

Fig. 6 shows a representative comparison between the automatic thickness measurement (left panels) and the manual thickness measurement (performed by one of the three operators - right panels) in rectus femoris (fig. 6.A – 6.B: 18.55 mm vs 19.23 mm), vastus lateralis (fig 6.C – 6.D: 20.69 mm vs 21.36 mm), tibialis anterior (fig 6.E – 6.F: 24.11 mm vs 23.96 mm), and medial gastrocnemius muscle (fig 6.G – 6.H: 18.33 mm vs 18.71 mm). The difference between the automatic and the manual measurement was in the range 0.15 – 0.68 mm (respectively: 0.68 mm for rectus femoris, 0.67 mm for vastus lateralis, 0.15 mm for tibialis anterior, 0.38 mm for medial gastrocnemius).

Similar to this example, analysis of the group data (Table 1) showed comparable results obtained by manual and automatic measurements. In fact, no significant differences between the former and the latter measurement were observed for both rectus femoris ($P=0.63$), vastus lateralis ($P=0.70$), tibialis anterior ($P=0.85$), and medial gastrocnemius ($P=0.23$).

The results of the ICC analysis are showed in Table 2: the agreement was excellent (range of ICCs: 0.98-0.99) for all muscles both among the three operators and between the manual and automatic measurements.

The Bland-Altman plot and the Spearman test showed (Fig. 7): (1) mean differences between the automatic and manual measurements in the range 0.06 – 0.45 mm and most of the differences between the 95% limits of agreement, thus suggesting that the two

measurement methods can be used interchangeably; (2) no significant correlation between the differences and means of the two measurements in each of the four muscles (rectus femoris: R= -0.08, P=0.55; vastus lateralis: R= -0.006, P=0.96; tibialis anterior: R= -0.15, P=0.29; medial gastrocnemius: R= -0.09, P=0.55), thus indicating that the accuracy of the automatic measurement was not related to the magnitude of the thickness value.

DISCUSSION

In the present study, we proposed a fully automatic method for the measurement of muscle thickness in musculoskeletal images acquired in the longitudinal plane (i.e., with the probe aligned to the direction of the muscle fibers).

Our automatic technique did not require any user interaction and it was capable of automatically detecting different muscles and delineating their superficial and deep aponeuroses in the whole database of 200 images (100% segmentation success rate).

The automatic detection of the aponeuroses in the ultrasound image is a challenging task. In fact, the muscle aponeuroses can be variable in shape and direction, and can also be located at different depth in the images, depending on different factors (subcutaneous adipose layer thickness, anatomy and contraction status of the muscle under study, age and health status of the investigated subject).

The observed robustness in the aponeuroses detection provided by MUSA is mainly due to the use of the FODG operator. In fact, this first-order derivative of the Gaussian kernel provides enhancement of the aponeurosis profiles without enhancing noise and with a very low computational burden. The size and σ values of the kernel were optimized to match the anatomical size of muscle aponeuroses.

The computational time depends on the image resolution, but in the current version of the method it is acceptable for both research investigations and clinical applications. The Matlab implementation of MUSA, which ran on a 3.1 GHz CPU, 8 GB RAM workstation, had an average computational time of 7.96 ± 3.04 s per image (6.40 ± 0.98 s for rectus femoris, vastus lateralis, and medial gastrocnemius images and 12.61 ± 2.24 s for tibialis anterior images). The most demanding task into the MUSA processing pipeline is the search for aponeurosis candidates that lead to the creation of the cleaned binary FODG mask, which required about 52% of the processing time (about 4.2 s).

The comparison between the automatic measurements and those manually performed by the three operators showed mean differences between the former and the latter measurements below 0.5 mm (0.45 mm in the worst case). Since the average muscle thickness was 22.9 mm (average of the thickness values provided by the three operators), the average measurement error was about 2% of the nominal muscle thickness. From a clinical point of view, this error can be considered negligible. In fact, a percentage reduction in muscle thickness in the range 5-10% is required to identify a condition of muscle hypotrophy, while a percentage reduction above 10% is required to identify a condition of muscle atrophy (Minetto et al. 2016).

We chose to study the four superficial muscles (rectus femoris, vastus lateralis, tibialis anterior and medial gastrocnemius) most informative for the investigation of neuromuscular disorders and sarcopenia (Abe et al. 2014; Minetto et al. 2016; Pillen et al. 2008). Future studies are required to test the accuracy of the MUSA algorithm for measuring the thickness of other skeletal muscles. However, from a technical point of view, our algorithm can be used to detect the aponeuroses of any muscle, provided that the

longitudinal projection is acquired. Figure 6 demonstrates that MUSA was accurate even on multi-compartment muscle, such as the tibialis anterior. To the best of our knowledge, MUSA is the first fully-automated system that can process images of muscles with multiple aponeuroses. Being totally automated, this system could also be used in future studies to initialize other techniques for the measurement of the muscle architectural parameters (such as muscle fascicle length and pennation angle) in single frames or in dynamic conditions.

CONCLUSION

To the best of our knowledge, MUSA is the first fully-automated system that can process images of different skeletal muscles, including the tibialis anterior that presents two compartments and three aponeuroses. The main results of the present study can be summarized as follows: i) the MUSA algorithm detected the aponeurosis profiles, and therefore automatically calculated the muscle thickness, in all muscle investigated; ii) the automatic and manual measurement methods could be used interchangeably: in fact, the mean differences between the automatic and manual measurements were below 0.5 mm (range 0.06 – 0.45 mm); iii) the accuracy of the automatic measurement was not related to the magnitude of the muscle thickness value.

ACKNOWLEDGEMENTS

The Authors are grateful to Dr. Diego Contro, Dr. Tommaso Menapace, and Dr. Rodolfo Zaottini (University of Turin, Italy) for their valuable assistance in image processing.

CONFLICTS OF INTEREST

The authors have no conflicts of interest.

REFERENCES

Abe T, Loenneke JP, Thiebaud RS. Ultrasound assessment of hamstring muscle size using posterior thigh muscle thickness. Clin Physiol Funct Imaging 2016;36:206–210.

Abe T, Loenneke JP, Young KC, Thiebaud RS, Nahar VK, Hollaway KM, Stover CD, Ford MA, Bass MA, Loftin M. Validity of Ultrasound Prediction Equations for Total and Regional Muscularity in Middle-aged and Older Men and Women. Ultrasound Med Biol 2015;41:557–564.

Abe T, Thiebaud RS, Loenneke JP, Loftin M, Fukunaga T. Prevalence of site-specific thigh sarcopenia in Japanese men and women. Age (Dordr) 2014;36:417–426.

Agyapong-Badu S, Warner M, Samuel D, Narici M, Cooper C SM. Anterior thigh composition measured using ultrasound imaging to quantify relative thickness of muscle and non-contractile tissue: a potential biomarker for musculoskeletal health. Physiol Meas 2014;35:2165.

Akagi R, Takai Y, Kato E, Wakahara T, Ohta M, Kanehisa H, Fukunaga T, Kawakami Y. Development of an equation to predict muscle volume of elbow flexors for men and women with a wide range of age. Eur J Appl Physiol 2010;108:689–694.

Arts IMP, Pillen S, Schelhaas HJ, Overeem S, Zwarts MJ. Normal values for quantitative muscle ultrasonography in adults. Muscle Nerve 2010;41:32–41.

Atkinson R a, Srinivas-Shankar U, Roberts S a, Connolly MJ, Adams JE, Oldham J a, Wu FCW, Seynnes

OR, Stewart CEH, Maganaris CN, Narici M V. Effects of testosterone on skeletal muscle architecture in intermediate-frail and frail elderly men. J Gerontol A Biol Sci Med Sci 2010;65:1215–1219.

Bland JM, Altman DG. A note on the use of the intraclass correlation coefficient in the evaluation of agreement between two methods of measurement. Comput Biol Med, 1990;20:337–340.

Caresio C, Molinari F, Emanuel G, Minetto MA. Muscle echo intensity: Reliability and conditioning factors. Clin Physiol Funct Imaging 2014;

de Boer MD, Seynnes OR, di Prampero PE, Pišot R, Mekjavić IB, Biolo G, Narici M V. Effect of 5 weeks horizontal bed rest on human muscle thickness and architecture of weight bearing and non-weight bearing muscles. Eur J Appl Physiol 2008. pp. 401–407.

Esformes JI, Narici M V., Maganaris CN. Measurement of human muscle volume using ultrasonography. Eur J Appl Physiol 2002;87:90–92.

Florack LMJ, ter Haar Romeny BM, Koenderink JJ, Viergever MA. Scale and the differential structure of images. Image Vis Comput 1992;10:376–388.

Han P, Chen Y, Ao L, Xie G, Li H, Wang L, Zhou Y. Automatic thickness estimation for skeletal muscle in ultrasonography: evaluation of two enhancement methods. Biomed Eng Online 2013;12:6.

Koo TKK, Wong C, Zheng Y. Reliability of Sonomyography for pectoralis major thickness measurement. Journal Manipulative Physiol Ther, 2010;33:386–394.

Ling S, Zhou Y, Chen Y, Zhao YQ, Wang L, Zheng YP. Automatic tracking of aponeuroses and estimation of muscle thickness in ultrasonography: A feasibility study. IEEE J Biomed Health Inform 2013;17:1031–1038.

Maganaris CN, Baltzopoulos V. Predictability of in vivo changes in pennation angle of human tibialis anterior muscle from rest to maximum isometric dorsiflexion. Eur J Appl Physiol Occup Physiol, 1999;79:294–297.

Minetto MA, Caresio C, Menapace T, Hajdarevic A, Marchini A, Molinari F, Maffiuletti NA.

Ultrasound-based detection of low muscle mass for diagnosis of sarcopenia in older adults. PM R, 2016;8:453–462.

Molinari F, Liboni W, Giustetto P, Badalamenti S, Suri JS. Automatic computer-based tracings (ACT) in longitudinal 2-d ultrasound images using different scanners. J Mech Med Biol World Scientific Publishing Co., 2009;09:481–505.

Narici M V., Flueck M, Koesters A, Gimpl M, Reifberger A, Seynnes OR, Niebauer J, Rittweger J, Mueller E. Skeletal muscle remodeling in response to alpine skiing training in older individuals. Scand J Med Sci Sport 2011;21:23–28.

Narici M V, Maganaris CN, Reeves ND, Capodaglio P. Effect of aging on human muscle architecture. J Appl Physiol 2003;95:2229–2234.

O. Duda R, E. Hart P. Use of the Hough transformation to detect lines and curves in pictures. Comm ACM 1971;15:11–15.

Ogawa M, Mitsukawa N, Bemben MG, Abe T. Ultrasound assessment of adductor muscle size using muscle thickness of the thigh. J Sport Rehabil 2012;21:244–8.

Otsu N. A threshold selection method from gray-level histograms. IEEE Trans Syst Man Cybern 1979;9:62–66.

Pillen S, Arts IMP, Zwarts MJ. Muscle ultrasound in neuromuscular disorders. Muscle Nerve 2008, 37, 679–693.

Saba L, Molinari F, Meiburger KM, Piga M, Zeng G, Rajendra Achraya U, Nicolaides A, Suri JS. What is the correct distance measurement metric when measuring carotid ultrasound intima-media thickness automatically? Int Angiol 2012;31:483–489.

Seynnes OR, Kamandulis S, Kairaitis R, Helland C, Campbell E-L, Brazaitis M, Skurvydas A, Narici M V. Effect of androgenic-anabolic steroids and heavy strength training on patellar tendon morphological and mechanical properties. J Appl Physiol 2013;115:84–9.

Sheehan FH, Bolson EL, Dodge HT, Mathey DG, Schofer J, Woo HW. Advantages and applications of

the centerline method for characterizing regional ventricular function. Circulation 1986;74:293–305.

Takai Y, Katsumata Y, Kawakami Y, Kanehisa H, Fukunaga T. Ultrasound method for estimating the cross-sectional area of the psoas major muscle. Med Sci Sports Exerc 2011;43:2000–2004.

Takai Y, Ohta M, Akagi R, Kato E, Wakahara T, Kawakami Y, Fukunaga T, Kanehisa H. Validity of ultrasound muscle thickness measurements for predicting leg skeletal muscle mass in healthy Japanese middle-aged and older individuals. J Physiol Anthropol 2013;32:12.

Takai Y, Ohta M, Akagi R, Kato E, Wakahara T, Kawakami Y, Fukunaga T, Kanehisa H. Applicability of ultrasound muscle thickness measurements for predicting fat-free mass in elderly population. J Nutr Health Aging 2014;18:579–585.

Wong A, Gallagher KM, Callaghan JP. Computerised system for measurement of muscle thickness based on ultrasonography. Comput Methods Biomech Biomed Engin 2013;16:249-255.

FIGURE CAPTIONS

Figure 1.

Schematic representation of the MUSA algorithm.

Figure 2.

MUSA algorithm first steps. (A) Original image of a representative medial gastrocnemius muscle; (B) Automatically cropped image; (C) Vertical Sobel of image; (D) Binary mask of the First-Order Derivative Gaussian (FODG) filter; (E) FODG mask with inconsistent aponeurosis structures eliminated; (F) FODG mask with branch removal. In panels E and F the arrow indicates the effect of the branch removal on the binary FODG mask.

Figure 3.

Fascicle detection and heuristic. (A) Binary mask obtained with image equalization and Otsu thresholding; (B) Cleaned fascicle mask; (C) Final fascicles mask overlaid on original image. The fascicles are portrayed in green, whereas the end points of the fascicles are in yellow; (D) Sketch of the heuristic search. The fascicles are shown in green, the end points in yellow, and three example ROIs are drawn in dotted rectangles.

Figure 4.

Final profile and correct aponeurosis determination. (A) Profile obtained at the end of the heuristic process. The white arrows indicates the presence of spikes; (B) Spikes removal and final trace of profile on the binary mask of the of the First-Order Derivative Gaussian (FODG) filter; (C) Application of the Difference of Gaussians (DoG) filter on the original image; (D) final interpolated profiles of the superficial and deep aponeuroses.

Figure 5.

Processing of tibialis anterior. (A) Example of tibialis anterior image; (B) Binary mask of the of First-Order Derivative Gaussian (FODG) filter for the tibialis anterior; (C) Profiles of the deep aponeurosis and of the central aponeurosis which define the deep compartment; (D) Profiles of superficial aponeurosis and of the central aponeurosis which define the

superficial compartment; (E) Final interpolated profiles of the superficial and deep aponeuroses for the tibialis anterior.

Figure 6.

Examples of automatic thickness measurement (left panels) and manual thickness measurement (performed by one of the three operators - right panels) in the four investigated muscles. APO_{SUP}: superficial aponeurosis, APO_{INF}: deep aponeurosis.

Figure 7.

Bland-Altman plots showing the comparison between the mean of the three operators and the automatic measurements for all four muscles considered: (A) rectus femoris, (B) vastus lateralis, (C) tibialis anterior, (D) medial gastrocnemius.

TABLES

Table 1

Muscle thickness measurements (mean ± SDs) obtained by each of the three operators and by MUSA algorithm for the four considered muscles.

Muscle	Operator 1 (mm)	Operator 2 (mm)	Operator 3 (mm)	MUSA (mm)
Rectus femoris	22.3 ± 3.8	22.4 ± 3.7	21.7 ± 3.7	21.8 ± 3.8
Vastus lateralis	21.9 ± 4.0	22.0 ± 4.0	21.4 ± 4.0	21.3 ± 4.0
Tibialis anterior	28.2 ± 3.6	28.0 ± 3.6	27.6 ± 3.5	27.9 ± 3.7
Medial gastrocnemius	19.9 ± 3.1	20.0 ± 3.0	19.3 ± 3.1	19.4 ± 3.1

Table 2

Intraclass correlation coefficient ICC (2,1) analysis.

Muscle	ICC (2,1) among the three operators	ICC (2,1) between the mean of three operators and the automatic measure
Rectus femoris	0.98	0.99
Vastus lateralis	0.99	0.99
Tibialis anterior	0.99	0.99
Medial gastrocnemius	0.98	0.99

Figure 1

Click here to download high resolution image

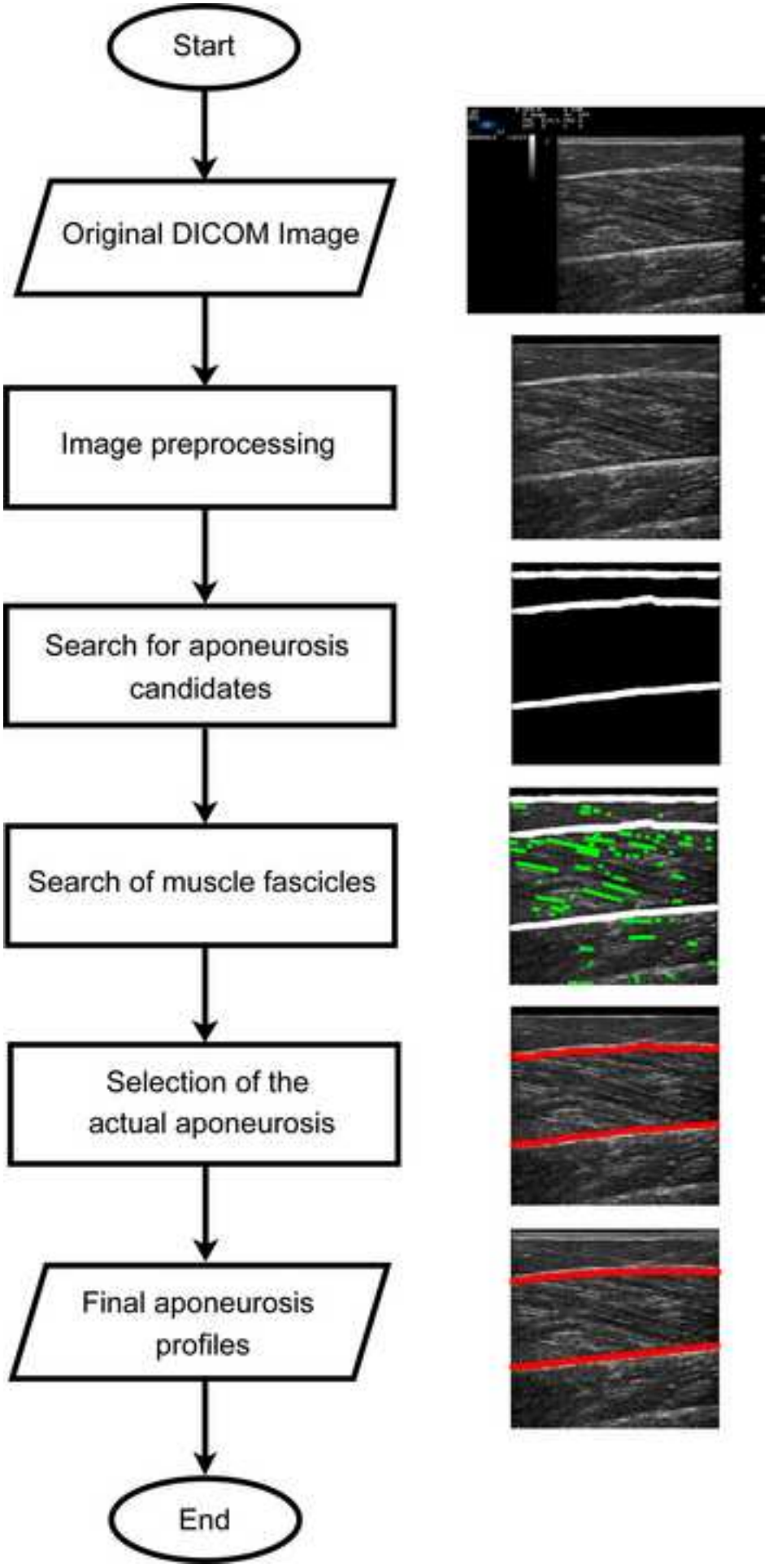

Figure 2

Click here to download high resolution image

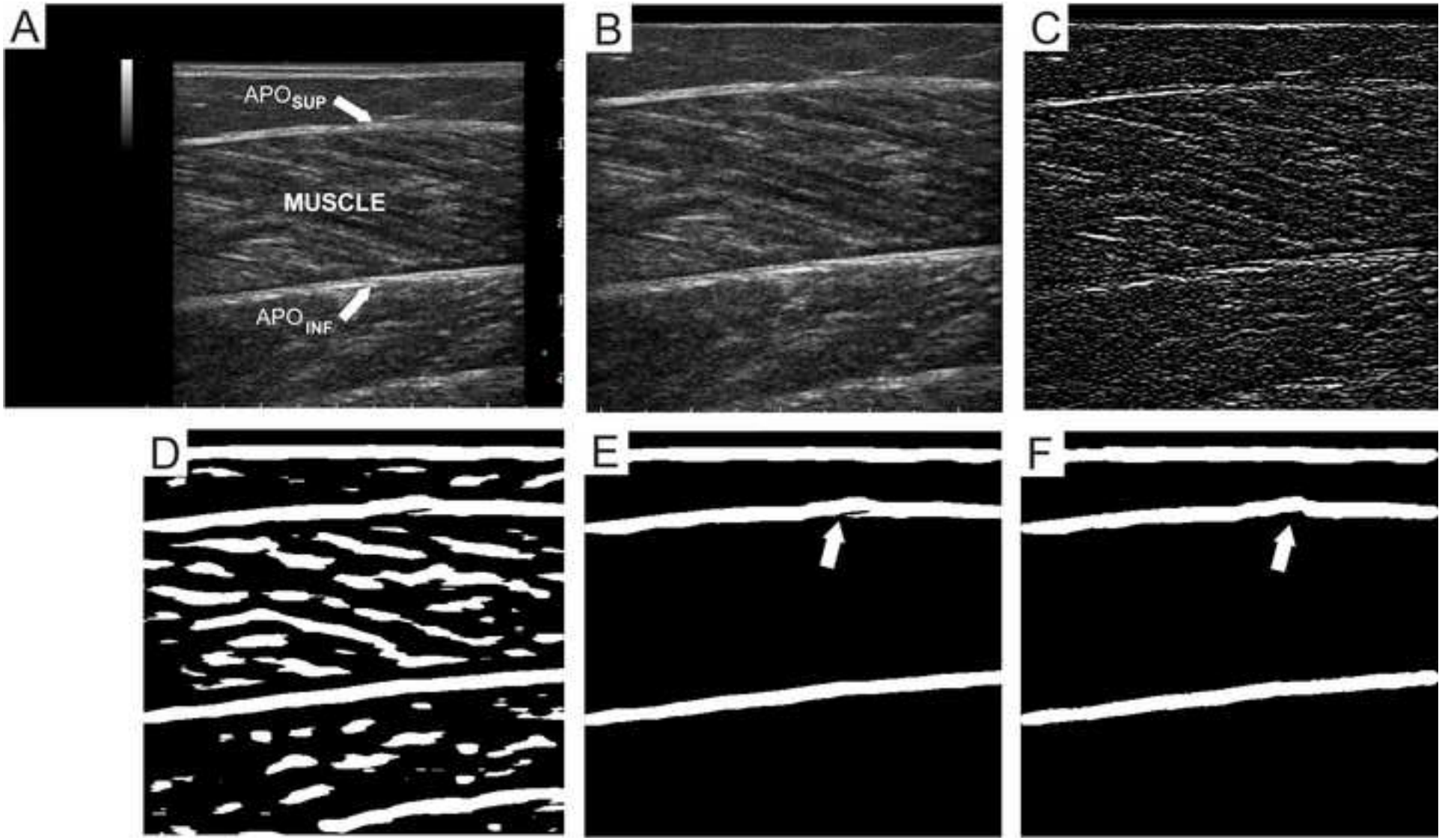

Figure 3

Click here to download high resolution image

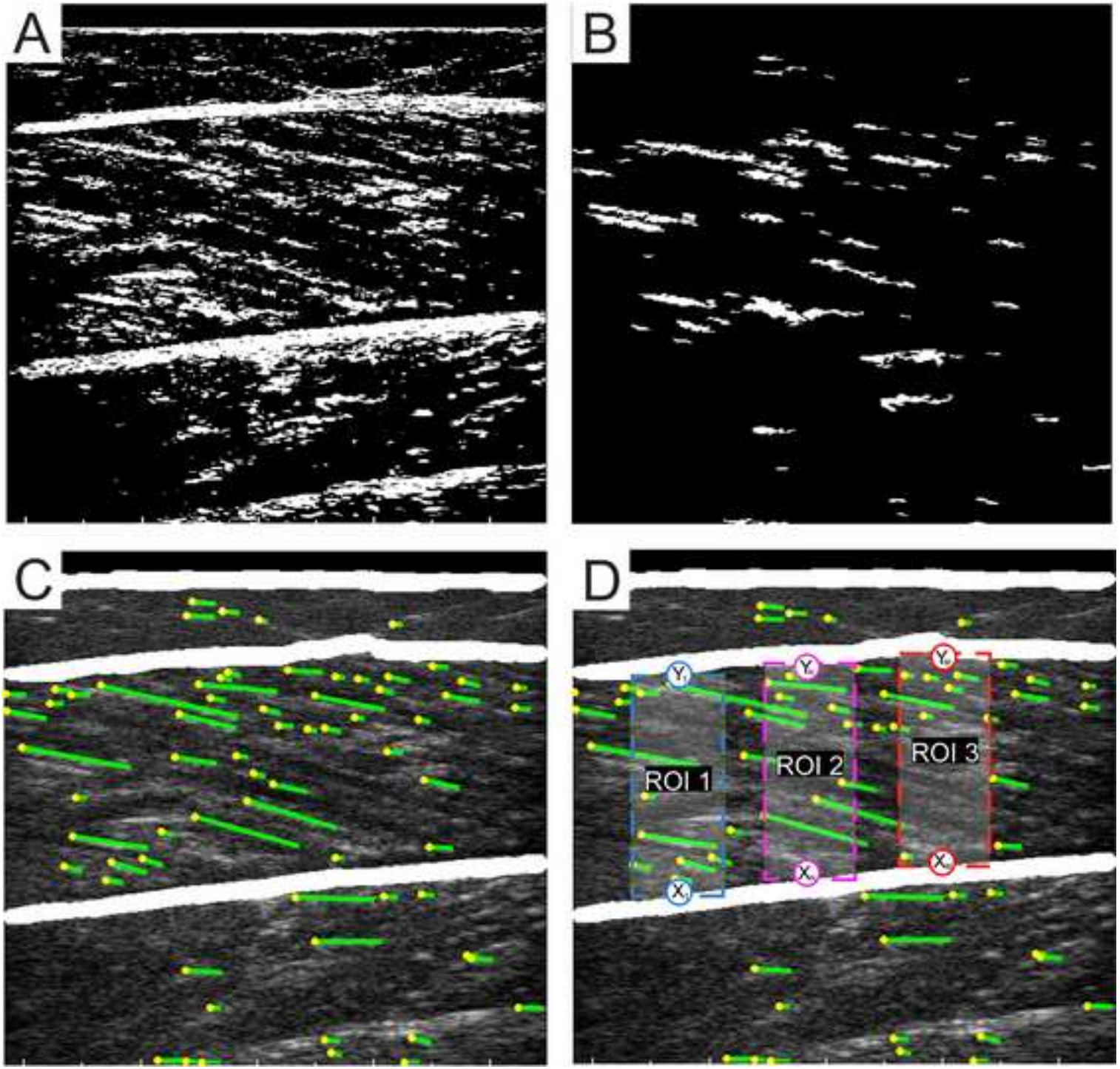

Figure 4

Click here to download high resolution image

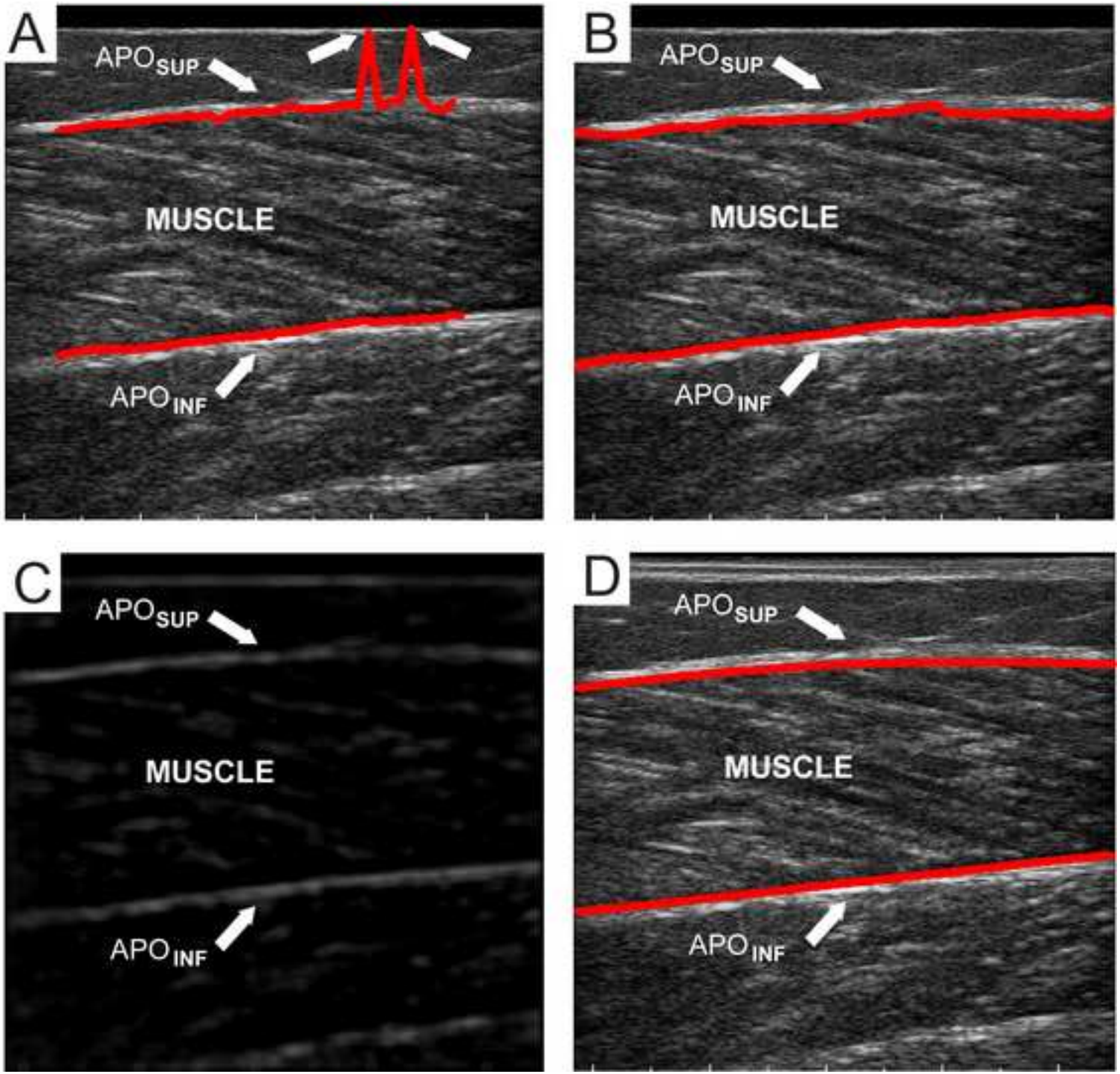

Figure 5

Click here to download high resolution image

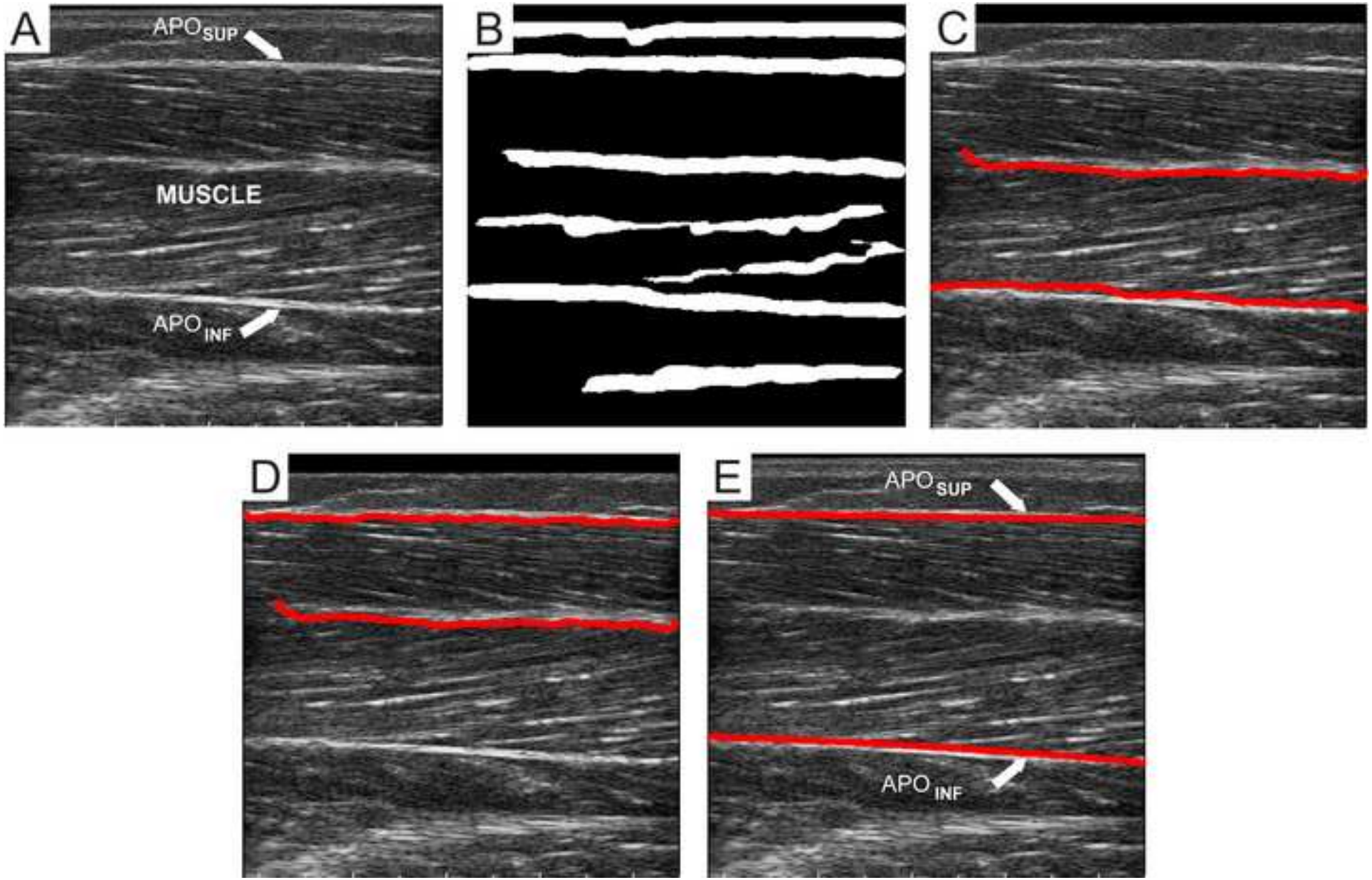

Figure 6

Click here to download high resolution image

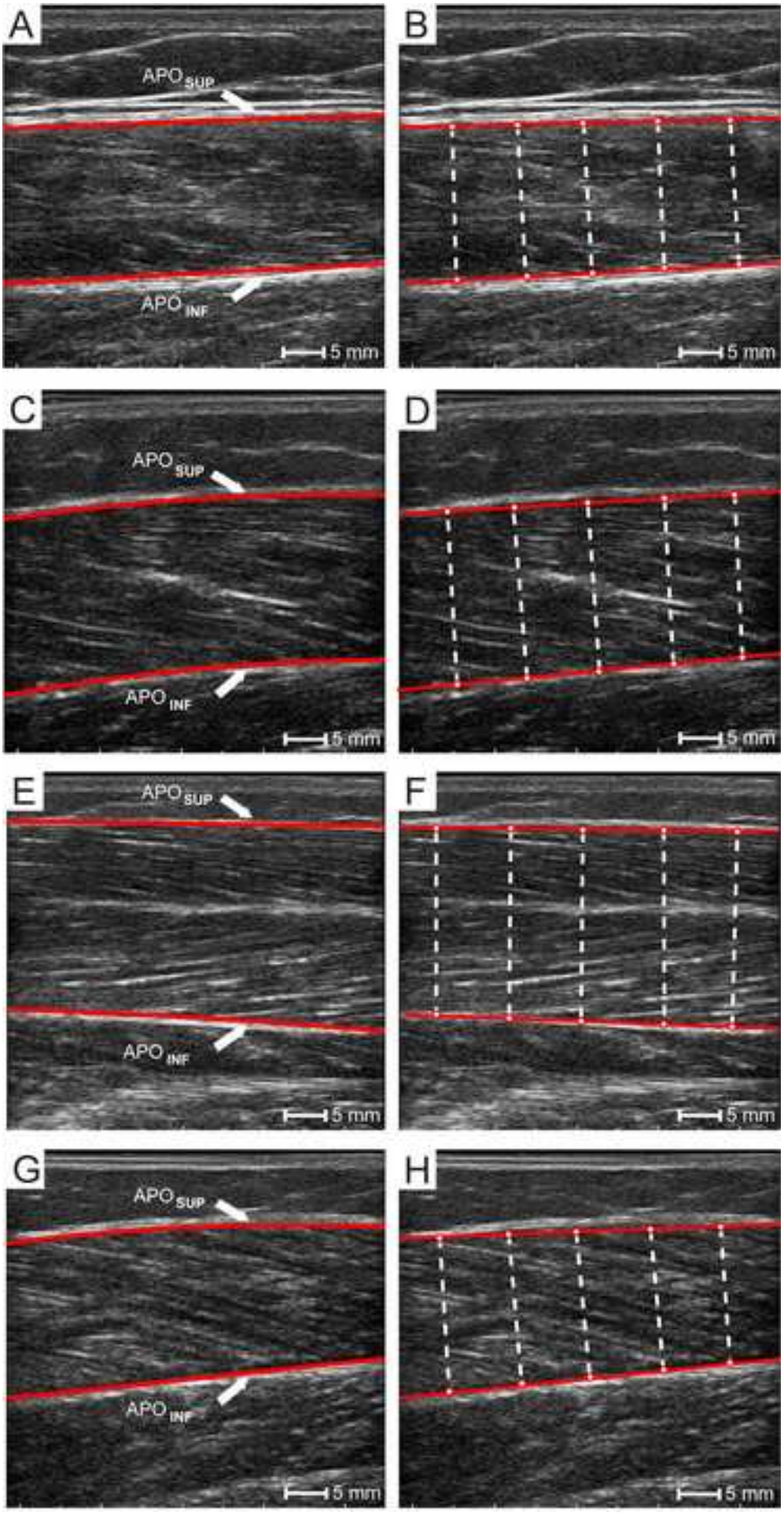

Figure 7

Click here to download high resolution image